Design and Analysis of MIMO Systems Using Energy Detectors for Sub-THz Applications

Simon Bicaïs, Alexis Falempin, Jean-Baptiste Doré, and Valentin Savin

***Abstract*—The significant amount of unused spectrum in sub-TeraHertz frequencies is contemplated to realize high rate wireless communications for beyond 5G networks. Yet, the performance of radio-frequency sub-TeraHertz systems is severely degraded by strong oscillator phase noise. Therefore, we investigate in this paper the use of multiple-input multiple-output (MIMO) systems with energy detection receivers to achieve high rate communications robust to phase noise. First, the design of the receiver detection algorithm is addressed. Two detectors are proposed for the studied nonlinear MIMO channel, either derived from the maximum likelihood decision rule by using a Gaussian approximation, or based on the use of neural networks. Second, the communication performance is assessed through numerical simulations for uncoded and coded systems. We consider a realistic scenario modeling an indoor wireless link in D-band with directive antennas and strongly correlated line-of-sight channels. Our results demonstrate that spatial multiplexing with non-coherent sub-TeraHertz transceivers can be realized on strongly correlated line-of-sight channels using the proposed detection schemes. Thereby, we highlight that high-rate radio-frequency sub-TeraHertz systems can be implemented with low-complexity and low-power architectures using MIMO systems with energy detection receivers.**

***Index Terms*—Sub-Terahertz communications, physical layer, MIMO, envelope detectors, detection algorithms, neural networks.**

I. Introduction

CONSIDERING the spectrum shortage in cellular bands, the interest for communications in the *TeraHertz* (THz) spectrum from 0.1 THz to 1 THz is continuously growing [2]. THz frequencies offer a significant amount of unused bands [3] and represent an opportunity to achieve high data rate wireless communications. Radio-frequency (RF) THz communication systems are envisaged to meet the requirements of beyond 5G networks. This paper focuses on the use of the sub-THz spectrum from 0.1 THz to 0.3 THz, in which bands of several tens of GHz are expected to be allocated to fixed and mobile services. In particular, we investigate one of the contemplated sub-THz applications [3]: a fixed indoor high data rate wireless link. Nonetheless, this paper provides general results relevant to other applications such as enhanced hot-spot *kiosk* or device-to-device communications.

To achieve high data rate sub-THz communications, additional research is required to design efficient and new physical layer algorithms. Traditional techniques cannot be directly transposed to sub-THz bands as they do not consider the specific features of RF impairments in sub-THz systems. In particular, they suffer from strong phase impairments due to the poor performance of high-frequency oscillators [4]. Indeed, as the carrier frequency increases, the phase noise performance of oscillators largely deteriorates. These strong phase impairments limit the achievable data rate of sub-THz systems, notably by causing detection errors. Therefore, state-of-the-art approaches [3], [5] investigate the use of coherent systems together with channel bonding, also referred to as carrier aggregation. This type of architecture needs to be further combined with signal processing optimizations [6], to mitigate the effects of phase impairments leading to complex practical implementations. Alternatively, one may consider the algorithm in [7] to mitigate the phase noise. Specifically, this algorithm allows to estimate and whiten the interference due to the phase impairments, based on the derivation of an approximate maximum likelihood detector. However, we consider in this study non-coherent detection, for its inherent robustness to phase noise and simple implementation. In contrast to the conventional approaches using linear RF chains, our purpose is to enable high-rate sub-THZ communications using low complexity transceivers, employing energy detectors and suitable transmission schemes. In this regard, it is worth mentioning that a fully integrated 260 GHz on-off keying (OOK) transceiver was demonstrated in [8]. Transceivers based on energy detection (ED) have been extensively studied for systems with a single transmit antenna and multiple receive antennas, see [9] and references therein. Nevertheless, for non-coherent sub-THz systems, the main challenge is to increase the spectral efficiency. With regard to this objective, the work in [10] is relevant as it shows that multiple-input multiple-output (MIMO) systems with amplitude detection receivers may exploit spatial multiplexing to increase their spectral efficiency. Therefore, we investigate the design of MIMO systems with ED receivers to achieve high rate sub-THz communications.

This paper extends the work in [10] by analyzing and evaluating the system performance in a sub-THz scenario. In contrast to [10], where the channel is built from independent and identically distributed (i.i.d.) Gaussian entries,

Manuscript received May 6, 2020; revised January 23, 2021, July 23, 2021, and October 15, 2021; accepted October 15, 2021. Date of publication November 2, 2021; date of current version June 10, 2022. This work was supported in part by the Electronic Components and Systems for European Leadership (ECSEL) Joint Undertaking Programme, under Grant N°826276 (CPS4EU Project). An earlier version of this paper was presented in part the 2020 IEEE International Symposium on Personal, Indoor and Mobile Radio Communications [DOI: 10.1109/PIMRC48278.2020.9217341]. The associate editor coordinating the review of this article and approving it for publication was S. Yang. *(Corresponding author: Jean-Baptiste Doré.)*

The authors are with the CEA-LETI, Université Grenoble Alpes, 38000 Grenoble, France (e-mail: jean-baptiste.dore@cea.fr).

Color versions of one or more figures in this article are available at https://doi.org/10.1109/TWC.2021.3123220.

Digital Object Identifier 10.1109/TWC.2021.3123220

we assume that each spatial stream is transmitted with a directive antenna on a line-of-sight (LoS) channel. Consequently, the channels are strongly correlated, and moreover, the resulting interference is nonlinear due to the ED at the receiver. The strong and nonlinear interference between channels represents a significant challenge to achieve spatial multiplexing gain with non-coherent transceivers in sub-THz frequencies. The contributions of the paper are the following. First, we derive an analytical model for MIMO systems using ED receivers in sub-THz bands. Second, the design of the receiver detection algorithm is investigated. We derive a detector corresponding to the studied nonlinear MIMO channel using a Gaussian approximation approach, which we refer to as the Maximum Likelihood Detector with Gaussian approximation (MLD-GA). In addition, we propose an original and efficient detector based on neural networks, which does not require any knowledge of the channel or assumption on it. We also detail the differences between state-of-the-art detection methods and the two proposed detectors. Third, the system performance is evaluated through numerical simulations. We introduce a realistic scenario modeling a fixed indoor wireless link in the D-band at 145 GHz. Our results show that communications can be achieved with strong spatial interference between channels using the proposed detection algorithms. Fourth, we consider the integration of a forward error correction (FEC) scheme in order to achieve channel coding gains. With regard to the targeted high-rate low-complexity applications, we propose the use of a Bose, Ray-Chaudhuri and Hocquenghem (BCH) code with a short packet length that can be implemented with a low-latency, low-complexity decoder. The results of numerical simulations confirm that the integration of the FEC scheme leads to significant performance gains in terms of achievable data rate. It should be mentioned that this work is an extension of our initial study [1] in which the system model and the detector have been introduced. In addition to [1], we conduct a more thorough analytical description. Moreover, we conduct a fine analysis of the detectors behavior through numerical simulations. We also present a practical implementation and the limitation of the mathematical system model. Notably, the practical radiation pattern of a real D-band antenna is considered and its performance is discussed and compared against the sectored antenna model, widely considered in the literature.

The main contribution of this paper is to demonstrate that spatial multiplexing with non-coherent sub-THz transceivers can be realized on strongly correlated LoS channels. Thereafter, this paper highlights that MIMO systems with ED receivers offer a valuable solution to achieve high rate communications in sub-THz frequencies with low-complexity and low-power RF architectures.

We also discuss the opportunity to derive a detector based on deep learning for such a nonlinear system model. Indeed, there has been a growing interest in wireless communications regarding the use of deep learning techniques for communications as it is addressed in [11], [12] and [13]. More specifically, [13] provides a general overview of the use of neural networks for detection in communication systems and also for linear MIMO systems. In [14], the use of deep neural network

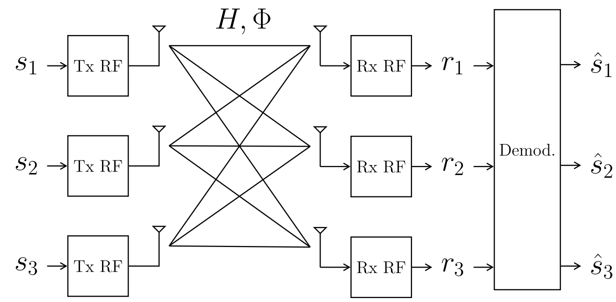

Fig. 1. Block diagram of a 3×3 MIMO transceiver.

detection is investigated for linear MIMO systems with the knowledge of the propagation matrices. In [15] and [16], the authors present neural network detectors both based on a linear MIMO system with channel and/or noise distribution knowledge. Nevertheless, none of these works consider the use of neural networks for nonlinear MIMO systems. Similarly to the proposed neural networks based detector, the combination of neural networks with energy detectors is addressed in [17]. However, in [17] neural networks serve a different purpose and aim to detect the unused portions of the spectrum in order communicate in an opportunistic way, *i.e.* spectrum sensing applications. To the best of authors' knowledge, the proposed neural network based detector for nonlinear MIMO system with ED receivers is original and not addressed in the literature. Finally, we also discuss the implementation of the proposed detection schemes in practical systems.

The remainder of this paper is structured as follows. Sec. II outlines the system model. In Sec. III, the design of the receiver detection algorithm is addressed. Sec. IV is dedicated to the performance analysis. Sec. V discusses several considerations related to the practical implementation of the proposed detectors. Eventually, Sec. VI concludes the paper.

II. System Model

We consider a MIMO communication system with N_t transmit antennas and N_r receive antennas with $N_t \leq N_r$, as illustrated in Fig. 1. The propagation channel is described by two $N_r \times N_t$ matrices: $\boldsymbol{H} = (h_{k,n})$ and $\boldsymbol{\Phi} = (\varphi_{k,n})$ where $h_{k,n}^2$ and $\varphi_{k,n}$ denote respectively the propagation gain and the phase shift of the channel for signals transmitted on the n-th Tx RF chain and received on the k-th Rx RF chain. To refer to this channel, we adopt hereafter the notation $n \rightarrow k$. In addition, it is of interest to express the propagation gain for channel $n \rightarrow k$ as $h_{k,n}^2 = g_{k,n}^{\mathrm{Tx}} \cdot l_{k,n} \cdot g_{k,n}^{\mathrm{Rx}}$ to highlight the influence of the antennas directivity gains $g_{k,n}^{\mathrm{Tx}}$, $g_{k,n}^{\mathrm{Rx}}$ and the path loss $l_{k,n}$. Column vectors $\boldsymbol{s} = [s_1 \ \ldots \ s_{N_t}]^\mathsf{T}$ and $\boldsymbol{r} = [r_1 \ \ldots \ r_{N_r}]^\mathsf{T}$ denote the sent and received symbols. Envelope modulation is used at the transmitter and ED at the receiver.

A. Transmitter RF Chain

The transmitter implements envelope modulation and the architecture of one of its RF chains is depicted in Fig. 2. Envelope modulation allows a simple implementation and an efficient use of power amplifiers. In this case, OOK appears to be a simple and efficient modulation scheme considering a non-coherent demodulation – see flash-signaling in [18]. On the n-th RF chain, we write $s_n(t) \in \mathbb{R}_{\geq 0}$ the modulating signal resulting from a rectangular pulse-shaping Π:

$$s_n(t) = \sum_{\tau \in \mathbb{Z}} s_n[\tau] \cdot \frac{\Pi\left(\frac{t}{T} - \tau - \frac{1}{2}\right)}{\sqrt{T}}, \quad t \in \mathbb{R}, \tag{1}$$

where $s_n[\tau]$ is the τ-th modulated symbol from constellation $\mathcal{C} = \{0, \sqrt{2}\}$ and T is the symbol duration. We have $\int_{\tau T}^{\tau T+T} |s_n(t)|^2 dt = s_n[\tau]^2$. The transmitted signal $x_n(t)$ at carrier frequency f_c is given by

$$x_n(t) = s_n(t) \cdot \sqrt{2}\cos(2\pi f_c t + \phi(t)), \tag{2}$$

where $\phi(t)$ is a stochastic process modeling a strong oscillator phase noise. The transmitter uses a single oscillator reference, common to all RF chains, hence the phase noise process $\phi(t)$ the same.

B. Propagation Channel

Recent measurement campaigns have shown that sub-THz propagation channels are largely dominated by a single path, often the LoS direct path, which provides most of the energy contribution [19], [20]. This is due to the stronger channel sparsity at those frequencies, in particular in open or urban environment, and to the usage of highly directive antennas, sometimes at both transceiver sides. The indoor radio propagation channel between 126 GHz and 156 GHz has been characterized in [19] and in [20] through measurements. Otherwise, the modeling of sub-THz channels is addressed in [21] using deterministic ray-tracing. Accordingly, we assume in this paper a static LoS channel model.

C. Receiver RF Chain

We detail here the receiver RF chains whose architecture is depicted in Fig. 2 for the k-th RF chain. The input of the k-th chain is the band-limited[1] signal $y_k(t)$, with bandwidth $B \geq 2/T$ centered around carrier frequency f_c. This signal is given by

$$y_k(t) = \sum_{n=1}^{N_t} h_{k,n} s_n(t) \sqrt{2}\cos\left(2\pi f_c t + \varphi_{k,n} + \phi(t)\right) + w_k(t), \tag{3}$$

where $w_k(t)$ is a band-limited continuous Gaussian process with spectral density N_0, modeling the thermal noise. To simplify further derivations, it is convenient to use the quadrature representation of the real thermal noise $w_k(t)$. Accordingly, $w_k(t)$ is represented using the real baseband signals $w_{k,c}(t)$ and $w_{k,s}(t)$ in quadrature and modulated at f_c. It follows that

$$w_k(t) = w_{k,c}(t)\sqrt{2}\cos(2\pi f_c t) - w_{k,s}(t)\sqrt{2}\sin(2\pi f_c t), \tag{4}$$

where $w_{k,c}(t)$ and $w_{k,s}(t)$ are band-limited continuous Gaussian process with spectral density $N_0/2$, $\varphi_{k,n} = d_{k,n} \cdot 2\pi f_c / c$ is the channel phase shift, with $d_{k,n}$ the propagation distance and c the light speed. The frequency

[1]The band-pass filter prevents the spectral folding of noise.

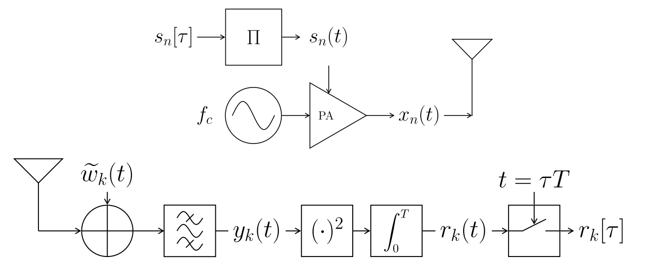

Fig. 2. Block diagram of one Tx-Rx chain.

down-conversion of the signal to baseband is achieved without impact of phase noise by squaring signal $y_k(t)$ and low-pass filtering it. That is

$$r_k(t) = \int_t^{t+T} y_k(u)^2 du, \tag{5}$$

with $f_c \gg 1/T$. For the k-th Rx RF chain, the τ-th received symbol $r_k[\tau] = r_k(\tau T)$ is obtained after integration and sampling, and can be expressed as

$$\begin{aligned} r_k[\tau] &= \sum_{n=1}^{N_t}\sum_{m=1}^{N_t} h_{k,n}s_n[\tau] \cdot h_{k,m}s_m[\tau]\cos(\varphi_{k,n} - \varphi_{k,m}) \\ &\quad +2\int_{\tau T}^{\tau T+T} w_{k,c}(t) \cdot \sum_{n=1}^{N_t} h_{k,n}s_n(t)\cos\left(\varphi_{k,n} + \phi(t)\right) dt \\ &\quad +2\int_{\tau T}^{\tau T+T} w_{k,s}(t) \cdot \sum_{n=1}^{N_t} h_{k,n}s_n(t)\sin\left(\varphi_{k,n} + \phi(t)\right) dt \\ &\quad +\int_{\tau T}^{\tau T+T} w_{k,c}(t)^2 + w_{k,s}(t)^2 dt. \end{aligned} \tag{6}$$

Regarding this equation, the first line represents the energy of the received signals of the different Tx chains whereas the following lines express the contribution of thermal noise in the received symbols. Accordingly, we denote the energy of the received signals

$$E_k[\tau] = \sum_{n=1}^{N_t}\sum_{m=1}^{N_t} h_{k,n}s_n[\tau]h_{k,m}s_m[\tau]\cos(\varphi_{k,n} - \varphi_{k,m}). \tag{7}$$

It should be noted that E_k expresses the nonlinear interference between the different channels of the system. Finally, we denote by $2M = \lfloor 2BT \rfloor + 1$ the time-bandwidth concentration of received signals [22], [23]. The time-bandwidth concentration is used in this paper to derive the probability distributions of received symbols. These derivations are detailed in the Appendix. It can be shown that the received symbols are given by

$$r_k[\tau] = E_k[\tau] + \sqrt{2E_k[\tau]} \cdot w_k[\tau] + z_k[\tau], \tag{8}$$

where $w_k[\tau] \sim \mathcal{N}(0, \sigma_w^2)$ is a zero-mean Gaussian variable with variance $\sigma_w^2 = N_0 B / 2M$ and $z_k[\tau] \sim \sigma_w^2/2 \cdot \chi_{4M}^2$ is a chi-square distributed variable with $4M$ degrees of freedom. Furthermore, Eq. (8) defines the nonlinear MIMO channel of the considered transceiver. In the following section, we investigate the design of the detection algorithm related to this channel. From now on, the time index τ is disregarded for brevity.

III. Detection Algorithm Design

A. Threshold Detector (TD)

We present in this paragraph the commonly used *threshold detector* abbreviated by *TD*. When using a single-antenna transceiver, this criterion has been shown to be optimal for the detection of an OOK with an ED receiver, *i.e.* minimizing the error probability [24]. This decision rule, defined upon a threshold comparison, can be expressed as

$$\hat{s}_k = \begin{cases} 0, & \text{if } r_k < \lambda_{\text{opt}}, \\ \sqrt{2}, & \text{otherwise.} \end{cases} \tag{9}$$

where λ_{opt} is the optimal threshold, and depends on $h_{k,k}^2$. This detector only requires the estimation of propagation gains $h_{k,k}^2$. The expression of λ_{opt} and its evaluation in practical systems are presented in [24]. Estimating symbol $\hat{s}_k$ on the k-th RF receiver chain, this detection criterion demodulates symbols from the different antennas independently. Using the TD in multiple-antennas systems implies the modeling of the spatial interference between channels as noise. On the one hand, if the spatial interference is negligible, this decision rule provides an efficient and low-complexity demodulation scheme. On the other hand, for strongly correlated channels, this detector might not be able to estimate sent symbols. In this case, a joint demodulation of the received symbols over all antennas should be used. We propose in the following paragraph a joint demodulation algorithm which exploits spatial interference between channels as information to demodulate symbols on strongly correlated channels.

B. Maximum Likelihood Detector With Gaussian Approximation (MLD-GA)

1) Position to State-of-the Art Techniques: Well-known for linear MIMO channels, the ML detector jointly demodulates the received symbols of the different RF chains. This detector uses spatial interference as information to demodulate symbols. It is important to point out unlike linear MIMO channels, the spatial interference between channels expressed in Eq. (7) is nonlinear due to the squaring of received signals such that traditional detectors cannot be used. Therefore, we derive here a sub-optimal detector corresponding to the nonlinear MIMO channel described in Eq. (8), using a Gaussian approximation approach. The proposed detector is further abbreviated by MLD-GA (Maximum Likelihood Detector with Gaussian Approximation). It should be mentioned that [10] also addresses the demodulation for a nonlinear MIMO system. In [10], the demodulation is based on amplitude detection of complex symbols resulting from a coherent receiver with a local oscillator. Consequently the demodulation proposed in [10] may be sensitive to phase impairments since the output of the matched-filter is subject to a penalty in signal-to-noise ratio (SNR) penalty, resulting from phase noise [25]. Conversely, we consider envelop extraction using energy detectors robust to phase noise. For this reason, the detector described in [10] cannot be used for the studied transceiver and differs from the proposed MLD-GA.

2) Derivation of the MLD-GA Decision Rule: For independent and equiprobable symbols, the ML decision rule is optimum, *i.e.* minimizes the error probability. It is defined upon the channel likelihood by

$$\hat{\boldsymbol{s}} = \underset{\boldsymbol{s}\in\mathcal{C}^{N_t}}{\arg\max}\; p(\boldsymbol{r}|\boldsymbol{s}, \boldsymbol{H}, \boldsymbol{\Phi}). \tag{10}$$

With regard to the superposition of χ^2 and Gaussian distributions in Eq. (8), the detection criterion resulting from the channel likelihood would be too complex to be evaluated in practical systems. To derive a decision rule with a simple implementation, we approximate the contribution of χ^2-distributed noise, precisely z_k in Eq. (8), by its expected value. The variance of z_k being $2M \cdot \sigma_w^4$, this approximation is tight at high SNR. Received symbol r_k then follows a Gaussian distribution

$$r_k \sim \mathcal{N}(\mu_k, \sigma_k^2), \tag{11}$$

where the mean and variance are given by

$$\mu_k = E_k + 2M \cdot \sigma_w^2, \tag{12}$$

$$\sigma_k^2 = 2E_k \cdot \sigma_w^2 + \varepsilon. \tag{13}$$

Though the noise contribution is approximated as Gaussian, the interference between channels remains nonlinear as expressed by E_k in Eq. (7). The term ε is introduced to prevent discontinuity[2] in the detection criterion. Then, the joint probability density function is given by

$$p(\boldsymbol{r}|\boldsymbol{s}, \boldsymbol{H}, \boldsymbol{\Phi}) = \prod_{k=1}^{N_r} \frac{1}{\sqrt{2\pi\sigma_k^2}} \exp\left(-\frac{|r_k - \mu_k|^2}{2\sigma_k^2}\right). \tag{14}$$

Finally, the detection decision rule can be written as

$$\hat{\boldsymbol{s}} = \underset{\boldsymbol{s}\in\mathcal{C}^{N_t}}{\arg\min} \sum_{k=1}^{N_r} \frac{|r_k - \mu_k(\boldsymbol{s})|^2}{\sigma_k(\boldsymbol{s})^2} + \ln\left(\sigma_k(\boldsymbol{s})^2\right). \tag{15}$$

This expression fully describes the proposed MLD-GA. The minimization space $\mathcal{C}^{N_t}$ increases exponentially with the number of antenna N_t. Since OOK modulation is used, the modulation order remains small, $|\mathcal{C}| = 2$, and the complexity of the MLD-GA algorithm is not an issue. It must be emphasized that the MLD-GA requires the estimation of $\boldsymbol{H}$ and $\boldsymbol{\Phi}$. The implementation of such estimation algorithm exceeds the scope of this paper and hence is not presented. In the following, we assume perfect knowledge of the channel at the receiver.

C. Neural Networks Based Detector (NND)

We now propose a novel and original *neural networks based detector* (*NND*) to estimate the sent symbols. The motivation of using neural networks is twofold. First, as discussed in the introduction, the considered system communicates through a nonlinear MIMO, and neural networks are efficient to solve multi-variables non-linear problems. Second, in the case of the MLD-GA algorithm, the impact of noise on received symbols is assumed to be Gaussian, assumption we do not make using

[2] Empirical results have shown that setting $\varepsilon = \sigma_w^2$ is an efficient choice to minimize the bit-error-rate.

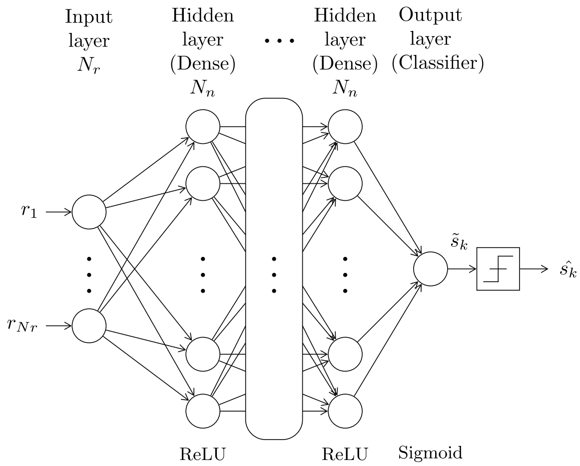

Fig. 3. Architecture of the k-th neural network of the NND.

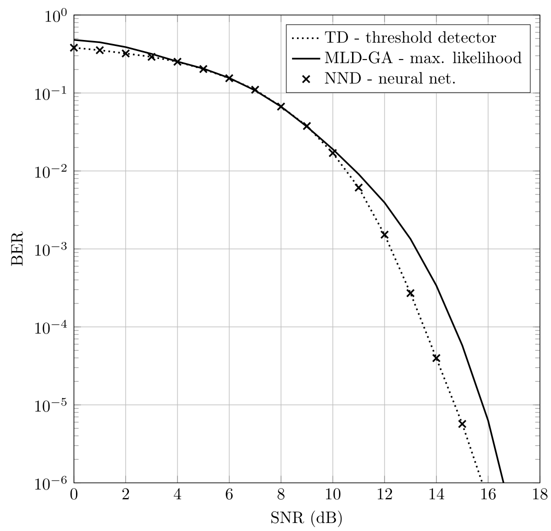

Fig. 4. Detection performance without spatial interference.

the NND. In addition, the NND does not explicitly need the propagation matrices $\boldsymbol{H}$ and $\boldsymbol{\Phi}$ to estimate symbols, as it learns the channel features during the training phase.

1) Architecture of the NND: The NND is composed of multiple neural networks estimating the transmitted symbols. It is worth noticing that the NND uses one neural network per transmit antenna. Each of the N_t neural networks estimates a single transmitted symbol. The proposed architecture of the k-th neural network is depicted in Fig. 3 for the detection of symbol s_k. This neural network uses fully connected hidden layers N_{hl}, each one composed of N_n neurons using rectified linear unit (ReLU) as activation function. The number of hidden layers is function[3] of the number of transmit antennas. The input layer has N_r units, each one representing a received symbol r_k. Finally, a prediction $\widetilde{s}_k$ – homologous to the probability $Pr(s_k = 0|\boldsymbol{r})$ – is produced at the output layer with a sigmoid unit. Thus, we build a multi-layer perceptron classifier in order to estimate the transmitted symbols s_k. Besides, it is worth mentioning that optimizing jointly the N_t neural networks is more complex, and we have not observed any performance improvement with respect to the parallel optimization. Therefore, we consider training each neural network independently in this paper. Eventually, the use of the NND is relevant for high-rate applications requiring parallel processing since sent symbols are estimated independently. Indeed, each neural network of the NND can be trained and provide inferences independently.

2) Training of the NND: The training of the NND is realized by transmitting some reference symbols known by the receiver. The set of weights is optimized during the training phase to maximize the detection performance of the NND. Each neural network, one per transmit antenna, is trained independently using an *Adam* (Adaptative Momentum estimation) optimizer [26]. The NND presents the advantage of having one loss function J_k to optimize per neural network. Since OOK modulation is exploited at the transmitter, it is pertinent to use a binary cross-entropy loss function J_k described by

$$-\frac{1}{B_s}\sum_{\tau=1}^{B_s}\left[\frac{s_k[\tau]}{\sqrt{2}}\ln\left(\widetilde{s}_k[\tau]\right)+\left(1-\frac{s_k[\tau]}{\sqrt{2}}\right)\ln\left(1-\widetilde{s}_k[\tau]\right)\right], \tag{16}$$

where B_s stands for the batch size. In addition, it may be noted that the fixed property of the wireless link in the targeted application is particularly suited to machine learning. Indeed, a calibration phase must be realized once the system is deployed because the received symbols depends on $\boldsymbol{H}$ and $\boldsymbol{\Phi}$. Moreover, the channel is assumed to vary slowly or even be static. Therefore we only need to train the NND once on pilot symbols. The spectral efficiency loss due to pilot symbols becomes insignificant because of the large channel coherence time for the envisaged scenarios. A detailed description of the NND implementation parameters is outlined in the following section presenting the results of numerical simulations.

IV. Performance Analysis

A. Systems Without Spatial Interference

To evaluate the performance of the detectors, we first investigate MIMO systems without spatial interference. The channels are perfectly spatially multiplexed, *i.e.* $\boldsymbol{H}$ is diagonal. To implement the TD decision rule in practical systems, the threshold λ_{opt} has to be evaluated efficiently. Therefore, we use the expression of λ_{opt} proposed in [24] using a polynomial approximation.

Fig. 4 presents the results of numerical simulations for systems using OOK with $N_t = N_r$ and no spatial interference. The communication performance is expressed in terms of bit-error-rate (BER) as a function of the SNR defined by $h_{k,k}^2/\sigma_w^2$. For transceivers without spatial interference, it can be shown that the NND achieves the optimal detection performance given by the TD. We can remark that the TD and the NND present a performance gain in comparison to the MLD-GA decision rule. The performance loss of the MLD-GA results from the Gaussian approximation of the channel. Indeed, in the

[3]We note that the choice of these parameters is empirical and we have observed for $N_t \leq 8$ some relations between the NND parameters and the system parameters such as $N_{hl} = N_t/2$ and $N_n = N_t^2$.

TABLE I
SIMULATION PARAMETERS

Parameters	Notation	Values
Carrier frequency	f_c	145 GHz
Symbol rate	$1/T$	1 GHz
Bandwidth	$B = 2/T$	2 GHz
Thermal noise	N_0	-174 dBm/Hz
Noise figure	N_f	10 dB
Antenna gain	g_0	32 dBi
Beam width	θ	3 °
Side lobe level	ϵ	-20 dB
Distance Tx - Rx	d_0	10 m

present case, considering a system without spatial interference equivalent to a single transmit antenna, the condition for the Gaussian approximation to be accurate, $\sigma_w^2 \ll E_k$, is not satisfied when transmitted symbol $s_k = 0$, since $E_k = 0$. Consequently, the MLD-GA is in this case sub-optimal. It is worth mentioning here that the MLD-GA is specifically designed for multi-antenna systems. The performance loss does not question the value of this detector, which is to be highlighted in the next paragraphs.

B. Scenario Description: Fixed Indoor Link in the D-Band

We introduce here a realistic sub-THz scenario. The targeted application is a fixed indoor wireless link in the D-band. Table I outlines the main simulation parameters for this scenario. The considered system uses a uniform linear array (ULA) of antennas with $N_t = N_r = N$. The disposition of the antennas is depicted in Fig. 5. The specification of the antenna is extracted from [27] which describes the design of a high-gain antenna for the D-band based on transmit-arrays. We evaluate the propagation gain $h_{k,n}^2/\sigma_w^2$ for channel $n \to k$ using the link budget given by the Friis' transmission equation. With $P_{\mathrm{A_{Tx}}}$ the transmit power per antenna, $G_{k,n}$ the antennas gain, and $d_{k,n}$ the propagation distance, the link budget is given by

$$\frac{h_{k,n}^2}{\sigma_w^2} = P_{\mathrm{A_{Tx}}} G_{k,n} \left(\frac{c}{4\pi f_c d_{k,n}}\right)^2 \left(\frac{N_0 B}{2M} N_f\right)^{-1}. \quad (17)$$

We have $G_{k,n} = g_{k,n}^{\mathrm{Tx}} \cdot g_{k,n}^{\mathrm{Rx}}$ the product of the Tx and Rx antennas directivity gains for channel $n \to k$. We assume the commonly used sectored antenna model illustrated in Fig. 5. The antenna directivity gain is then defined by

$$g(\alpha) = \begin{cases} g_0, & \text{if } |\alpha| < \frac{\theta}{2}, \\ g_0 \cdot \epsilon, & \text{otherwise}, \end{cases} \quad (18)$$

depending on the beam width θ, the beam offset angle to the main lobe α, the side lobe level ϵ ($0 < \epsilon \ll 1$) and the antenna gain g_0. The considered scenario is symmetric and the beam of the k-th transmit antenna is aligned with the k-th receive one. This leads to $g_{k,n}^{\mathrm{Tx}} = g_{k,n}^{\mathrm{Rx}} = g(\alpha_{k,n})$ with $\alpha_{k,n}$ the beam offset angle for channel $n \to k$. Eventually, the channel matrix $\boldsymbol{H}$ may be evaluated using Eq. (17) and Table I. The maximum propagation gain $h_{k,k}^2$ is achieved for any channel $k \to k$. For a transmit power per antenna $P_{\mathrm{A_{Tx}}} = -30$ dBm, we have

$$\mathrm{SNR} = \frac{h_{k,k}^2}{\sigma_w^2} \simeq 16.23 \text{ dB}. \quad (19)$$

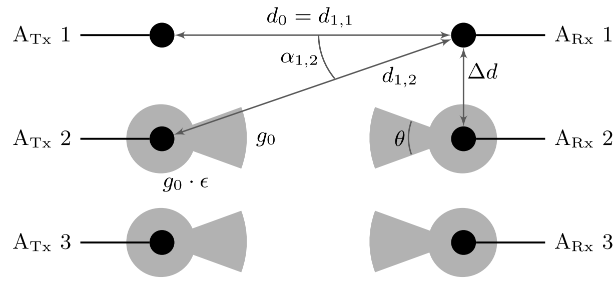

Fig. 5. Disposition of the antennas in the scenario.

For $k' \neq k$, the interference terms (off-diagonal elements) in matrix $\boldsymbol{H}$ are approximately

$$\frac{h_{k,k'}^2}{h_{k,k}^2} \simeq \begin{cases} -0.01 \text{ dB}, & \text{if } |\alpha_{k,k'}| < \frac{\theta}{2}, \\ -40.02 \text{ dB}, & \text{otherwise}. \end{cases} \quad (20)$$

When $\Delta d \ll d_0$ the differences in path loss between channels are close to zero. Subsequently, the level of interference between two channels, either strong 0 dB or very low -40 dB, only results from the angle $\alpha_{k,k'}$. If the inter-antenna distance Δd is sufficiently large,

$$\Delta d \geq d^* = d_0 \tan\left(\frac{\theta}{2}\right), \quad (21)$$

the channels are almost perfectly spatially multiplexed. In this case, the interference results from side lobes of the antennas and is very low (< -40 dB). This corresponds closely to an ideal case and the system performance for any N equals the one described in Fig. 4 without interference. Since $d^* \simeq 26$ cm, the latter condition implies that the width ℓ of the array of antennas may be significantly large for practical implementation. The width of the ULA $\ell = d_{\mathrm{A}} + (N-1)\Delta d$, where $d_{\mathrm{A}} = 5$ cm is the width of the antenna itself [27]. By way of illustration, for $N = 8$ we have $\ell > 1.8$ m. To reduce the width of the transceiver, we now consider a smaller inter-antenna distance satisfying

$$d^* \frac{2}{\kappa - 1} \; > \; \Delta d \; \geq \; d^* \frac{2}{\kappa + 1}, \quad (22)$$

where $\kappa \in \{3, 5, \ldots, 2N-1\}$. In this case, the main lobe of one transmit antenna beam enlightens multiple receive antennas, namely up to κ. Put differently, κ denotes the maximum number of transmitted symbols strongly interfering on a receive antenna. Hence, the larger the value of κ, the stronger the spatial interference between channels. By means of illustration, the channel gain matrix $\boldsymbol{H}$ for $N = 4$ and $\kappa = 3$ may be accurately approximated[4] as follows

$$\boldsymbol{H} \simeq h_{1,1} \cdot \begin{bmatrix} 1 & 1 & \rho & \rho \\ 1 & 1 & 1 & \rho \\ \rho & 1 & 1 & 1 \\ \rho & \rho & 1 & 1 \end{bmatrix}, \quad (23)$$

where ρ is the residual interference due to side lobes of the antennas with $\rho^2 = -40$ dB. There are κ diagonals whose

[4]Since the differences in path loss is less than 0.02 dB, the adjacent channels interference and the residual side lobes interference can be respectively approximated to 1 and a constant ρ.

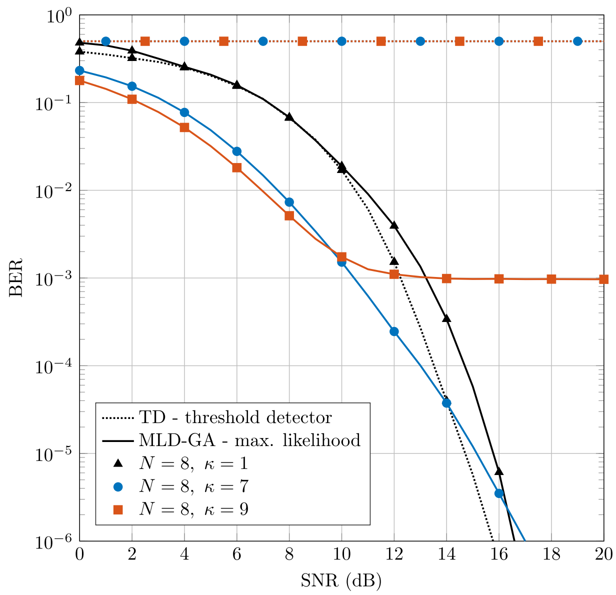

Fig. 6. Influence of the level of spatial interference (parameter κ) on the system performance. Solid lines are for the MLD-GA while dashed line for the threshold detector.

elements are 1 which equals the maximum number of interfering symbols on a receive antenna. We use hereafter $\kappa = 1$ to denote the multiplexed case corresponding to Eq. (21). Eventually, parameter κ enables us to quantify the level of spatial interference.

C. Systems With Strong Spatial Interference

We now evaluate the influence of the spatial interference on the system performance, using parameter κ. In these simulations, the propagation gain and the phase shift matrices are not approximated, but are exactly computed from the scenario description and simulation parameters.

1) MLD-GA vs. TD: The results of numerical simulations comparing the detection performance of the MLD-GA and the TD are depicted in Fig. 6. The BER performance is assessed for $N = 8$ and different values of κ. First, it must be emphasized that the MLD-GA is essential to communicate on strongly correlated channels. As expected for $\kappa > 1$ the TD cannot demodulate sent symbols and presents a BER of $1/2$. Nevertheless, we can remark that if the spatial interference is too strong, *e.g.* $\kappa = 9$ in Fig. 6, the BER reaches an error floor. Simulation results also show that in the moderate SNR regime, transceivers with large values of κ, *i.e.* strong spatial interference, may demonstrate lower BER than the multiplexed case $\kappa = 1$. With channel coding, such property may be beneficial for configurations with κ large. If the BER is low enough, the waterfall feature of the decoding algorithm may be exhibited at a lower SNR. Subsequently, setting κ large is interesting to achieve low error rate communications with the combination of a channel coding while reducing the width of the transceiver. The properties exhibited for $N = 8$ in Fig. 6 also hold for different values of N.

2) MLD-GA vs. NND: This paragraph presents the communication performance of the NND and the MLD-GA algorithms on strongly correlated LoS channels. Table II presents the parameters of the NND architecture for the different system configurations. The training dataset contains about 10^6 symbols when using a 8×8 MIMO system. These symbols are used to train the 8 neural networks estimating each one a transmitted symbol. The neural networks are trained independently using 50 to 150 epochs. For the simulations presented in this paragraph, NND is trained on Graphics Processing Unit (GPU) processor and infered on Central Processing Unit (CPU) processor. However, in a practical system, for fixed indoor links, a calibration phase is needed using pilot symbols. These pilot symbols could be sent to a cloud to perform the training phase for example. Then, the NND would be infered in an embedded system using an ASIC (Application-Specific Integrated Circuit) or a FPGA (Field-Programmable Gate Array) circuit. Here the tuning of the NND parameters is empirical, yet we can admit that increasing the number of antennas induces an increase of the number of hidden layers and neurons. The results of numerical simulations are depicted in Fig. 7 and Fig. 8. The BER performance is assessed for $N = 4$ and $N = 8$ and different values of κ, *i.e.* different levels of spatial interference. First, we can notice that, for $\kappa = 1$ with any number of antennas N, the performance equals the one without interference described in Sec. IV-A. It can be noticed in Table II that there is no hidden layer for the case without interference. Indeed, only one neuron with sigmoid output is sufficient. Second, for $N = 4$ with spatial interference, it can be observed that the MLD-GA and the NND present similar detection performance. Though, the NND demonstrates slight performance gains. Nonetheless, it should be noted that if the spatial interference is too strong, *e.g.* $\kappa = 5$ for $N = 4$ or $\kappa = 9$ for $N = 8$, the BER reaches an error floor. Third, for $N = 8$, we notice that the system performance of the NND is close to the one of the MLD-GA if the spatial interference is not too strong. With strong interference, $\kappa = 9$ and $N = 8$, using the NND leads to a significant performance loss. Moreover, at low SNR, the MLD-GA uses a Gaussian approximation whereas the NND does not. Therefore, it explains why the NND is generally better than the MLD-GA. However, this property is not verified for $\kappa = 9$ due to high level of spatial interference. The current NND architecture has difficulties to cope with high interference level which explains the lack of performance for the case $\kappa = 9$. Further investigations regarding the architecture and the learning are expected to reduce the performance loss. It should also be mentioned that increasing the number of neurons in that case does not induce performance gain, meaning that with this architecture we may not expect better performance for $\kappa = 9$ and $N = 8$.

D. Discussions

We conclude this section on the analysis of the system performance analysis by discussing some properties of the transceiver. First, and similarly to linear MIMO systems, the considered system benefits from the spatial diversity. Sent symbols of a transmit-antenna may be received on several receive-antennas. This property thus improves the robustness to thermal noise. It explains the performance gains achieved by systems with strong interference in the moderate SNR regime in comparison to the multiplexed case, for instance as

TABLE II
NND PARAMETERS

Parameters	**MIMO no interference**	4×4 **MIMO**	8×8 **MIMO**
Hidden layers (HL)	0	2	4
Neurons/HL	–	16	64
Batch size	32	32	256
Dataset size	10^5 symbols	10^6 symbols	
Epochs	50	150	150
Optimizer	Adam		
Learning rate	0.001		
Loss function	Binary cross-entropy Eq. (16)		
Activation functions	ReLU and Sigmoid		

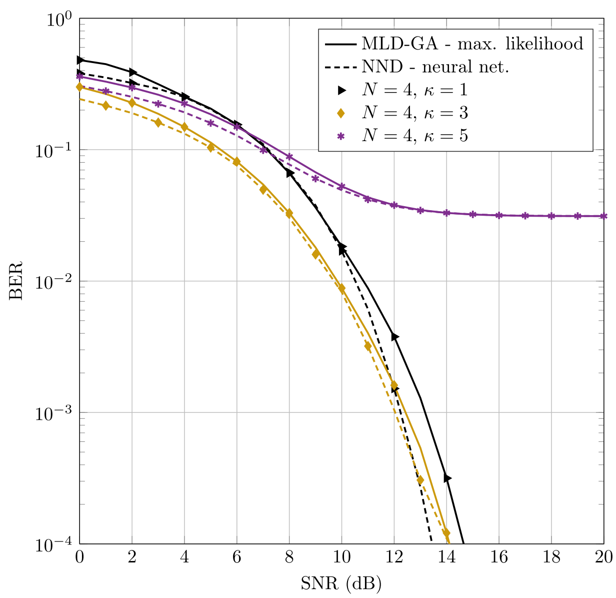

Fig. 7. Performance of the MLD-GA and the NND for $N = 4$. Solid lines are for the MLD-GA while dashed lines for the NND.

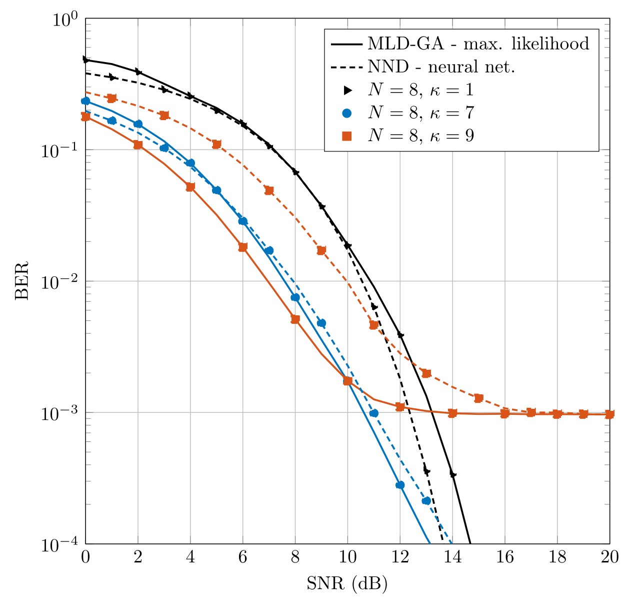

Fig. 8. Performance of the MLD-GA and the NND for $N = 8$. Solid lines are for the MLD-GA while dashed lines for the NND.

shown in Fig. 6. In addition to diversity, the studied system is also subject to ambiguity. Since the communication channel is a nonlinear MIMO channel, different transmitted MIMO symbols $\boldsymbol{s}$ may lead to similar received observations $\boldsymbol{r}$. For this reason, the BER of system configurations with strong spatial interference reaches an error floor, *e.g.* $\kappa = 5$ for $N = 4$ in Fig. 7 or $\kappa = 9$ for $N = 8$ in Fig. 8. Subsequently, we claim that the level of spatial interference, and hence the inter-antenna spacing Δd, is directly related to a trade-off between diversity and ambiguity. Second, it is also worth mentioning that significant differences in channel qualities exist. The different spatial streams – corresponding to a pair of aligned transmit and receive antennas – are not subject to the same interference. As illustrated by Eq. (23), the numbers of symbols strongly interfering is larger for the receive antennas in the middle of the ULA than for the antennas on the extremities. Consequently, the interference is stronger for the antennas in the middle of the ULA than the ones on the extremities. We will see in the next section that this property can be exploited by the channel coding scheme to enhance the system performance by adaptive coding rate selection. In all our numerical simulations, we assume that the antennas are perfectly aligned. In case of misalignment, the entire system model and algorithms remain valid. The misalignment effect will be captured by the channel estimation scheme for the MLD-GA and by the learning mechanism for the NND. Finally, our results demonstrate that spatial multiplexing with non-coherent sub-THz transceivers can be realized on strongly correlated LoS channels. MIMO systems with ED receivers hence offer a valuable solution to achieve high rate communications in sub-THz frequencies. Since the analysis is carried out with some approximations, in particular on the antenna model, the exactitude of the conclusions could be questioned. Nevertheless, the next section proposes to improve the performance analysis by considering and discussing some practical implementation issues.

V. IMPLEMENTATION CONSIDERATIONS

We have previously shown that low-complexity low-power transceivers using MIMO systems with energy detection receivers can be implemented within sub-THz frequencies. In this section, we first evaluate the system performance with the real antenna radiation pattern from [27]. Second, we consider the integration of a forward error correction (FEC) scheme as channel coding. Third, the practical implementation of the proposed detection schemes is discussed.

A. Performance With the Real Antenna Gain

Previously, we have based the performance analysis upon the commonly used sectored antenna model. The sectored

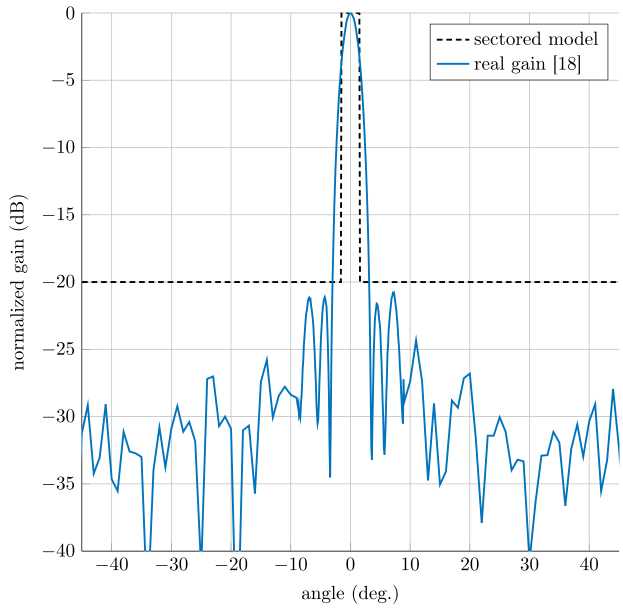

Fig. 9. Antenna gain measured in [27] (normalized to 32 dBi).

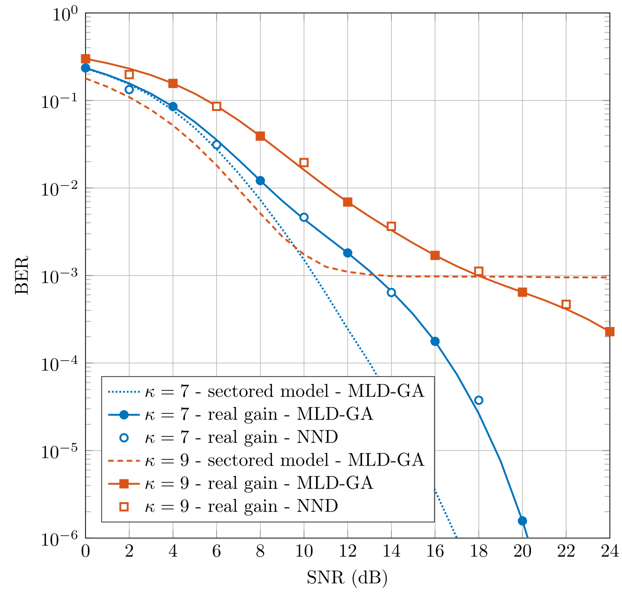

Fig. 10. Performance for $N = 8$ with the real antenna gain.

model is relevant for its simple analytic expression. However, the accuracy of the analysis can be improved by considering the real antenna radiation pattern measured and published in [27]. Fig. 9 depicts the real antenna radiation pattern and the sectored model. The assessment of communication performance with the real antenna gain, in comparison to the sectored model, is presented in Fig. 10 for $N = 8$ and using the MLD-GA and the NND. It can be observed that the BER performance of system configurations with strong interference is deteriorated when the real antenna gain is considered. Specifically, the performance are worse at low SNR for the real antenna radiation pattern. The performance loss can be explained by a loss of diversity due to lower side lobes. However, it should be emphasized that the error floor is removed. With the real radiation pattern, sent symbols are received on multiple antennas but with lower energy than with the sectored pattern. Nevertheless, and conversely to the sectored model, it can be noted that ambiguity is removed and thus no error floor is observed with the real antenna radiation pattern, see the configuration $N = 8$, $\kappa = 9$. In addition, it should be emphasized that the MLD-GA and the NND demonstrate similar demodulation performance in the case of the real antenna gain. We conclude from these results that the sectored antenna model is an efficient but mostly optimistic model to describe practical systems. In the following, any further performance analysis is based on the real radiation pattern of the antenna directivity gain.

B. Performance With Channel Coding

We have previously demonstrated the influence of the level of spatial interference (parameter κ) on the system performance. It can be observed that the waterfall BER performance is improving with increasing κ. However, when κ increases too much, the BER may reach an error floor (e.g., $\kappa = 9$, the BER reaches an error floor at 10^{-3}). Yet, for a coded system such an error floor may be lowered or even removed by the FEC scheme. Therefore, it is interesting to consider the integration of a FEC scheme to achieve channel coding gain and low error rates. However, implementing the FEC, and in particular its decoder, may entail a significant complexity and power consumption. To achieve a low-complexity low-power transceiver, we propose here to use a BCH code. The considered FEC scheme is a BCH code with a packet size of 63 bits and a coding rate ranging from 0.4 to 0.9. We consider a hard-input, syndrome-based, half the minimum distance bounded decoding algorithm. It should be mentioned that the key features of this code are a low-complexity implementation and a low-power consumption [28]. In addition, with regard to the short packet size, this code has a low-latency decoder. These features appear to be highly relevant for the scenario investigated in this paper. The considered transceiver architecture with the integration of a channel coding is presented in Fig. 11. Multiple FEC schemes are used and the coding rate can be adapted to the channel quality of the receive antenna. Since the channel is assumed to be static, channel coding with adaptive rate is implemented only to adapt the coding rate to the receive antenna. Indeed, the channel presents significant differences in terms of quality depending on the receive antenna. Receive antennas in the middle of the ULA are subject to stronger interference than the ones on the extremities. For this reason, adapting the coding rate to the receive antenna enables us to capitalize on the latter property to further enhance demodulation performance. The system architecture in Fig. 11 is particularly interesting as it also maintains a high degree of parallelism.

Fig. 12 presents the achievable rates as function of E_b/N_0B for systems with a BCH code such that the BER is below 10^{-6}. The BCH code is implemented with a coding rate ranging from 0.4 to 1 and a channel decoder based on the hard decisions produced by the MLD-GA. Numerical results have been obtained through Monte-Carlo simulations with the

TABLE III
SYNTHESIS OF THE MAIN SYSTEM PARAMETERS AND KEY PERFORMANCE INDICATORS

Carrier frequency	f_c	145 GHz			
Bandwidth	B	2 GHz			
Propagation distance	d_0	10 m			
Antenna gain	g_0	32 dBi			
Number of antennas	N	1	4	6	8
Throughput	$N/T \cdot 0.9$	0.9 Gbps	3.6 Gbps	5.4 Gbps	7.2 Gbps
Power by antenna	$P_{\mathrm{A_{Tx}}}$	-31.8 dBm	-31.2 dBm	-30.4 dBm	-32.3 dBm
Width of the ULA	ℓ	5 cm	44 cm	50 cm	55 cm
Inter-antenna distance	Δd	$\varnothing$	13 cm	9 cm	7 cm

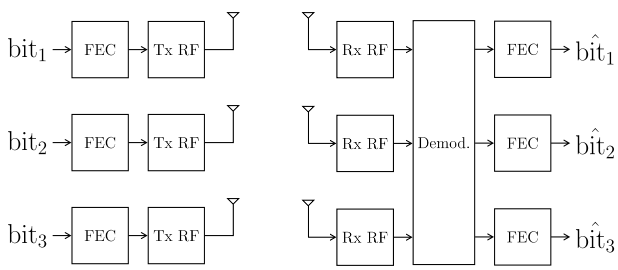

Fig. 11. System architecture integrating a FEC scheme.

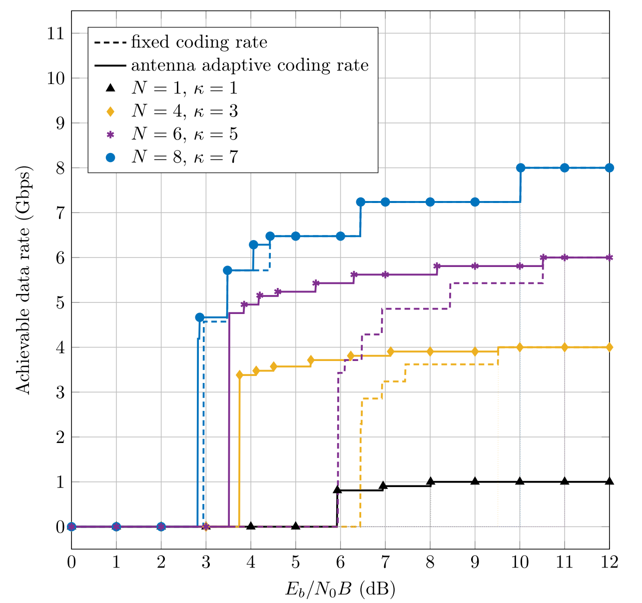

Fig. 12. Achievable data rate with a BCH code and the real antenna gain. The dashed lines are for a scheme with fixed coding rate and the solid lines for the achievable data rate with an adaptive coding rate strategy.

real antenna radiation pattern. First, it should be remarked that integrating a FEC scheme enables to achieve a significant channel coding gain. Second, it can be noticed that the adaption of the coding rate to the receive antenna leads to performance gains in comparison to setting a fixed coding rate for all antennas. In particular, we can see that for $N = 4$ and $N = 6$ the performance gains are larger than 2 dB.

To present the results of Fig. 12 differently, we propose in Table III a synthesis of the system performance and parameters for different number of antennas. For all system configurations, the system bandwidth is $B = 2$ GHz, the distance Tx-Rx is $d_0 = 10$ meters, and the coding rate of the BCH is 0.9. Though the system performance is evaluated with the MLD-GA, similar results are expected using a demodulation based on the NND. Further, a channel bonding scheme, aggregating several sub-bands, could increase the throughput and allow to benefit from the large available free spectrum offered in sub-THz bands. It can be concluded that MIMO systems using ED receivers may achieve high rate communications in sub-THz bands with low-power and low-complexity RF architectures. Performance of coded systems could be further improved by considering longer packet length, soft-decision channel decoding, or capacity-achieving codes, *e.g.* a polar code, yet at the detriment of complexity.

C. Comparison of the Proposed Detection Algorithms

This section provides an overview of practical aspects of MLD-GA and NND techniques, to understand their respective benefits and drawbacks.

1) Channel Estimation: The first difference between the MLD-GA and NND is the following. To perform its decision rules, the MLD-GA algorithm requires an explicit knowledge of H, σ_w and Φ, and hence, also the design of a channel estimation algorithm. In contrast, the NND is able to learn the channel features, and implicitly the channel matrices, during the training phase in order to demodulate the received symbols. The transmission of reference symbols is required for both detection algorithms which results in a spectral efficiency loss.

2) Algorithmic and Implementation Complexity: The computational complexity of MLD-GA and NND algorithms can be estimated. Yet, from an implementation perspective, it is delicate to draw conclusions based on the computational complexity only, as these algorithms lie in different paradigms. The MLD-GA algorithm is a common detection method. Although the complexity of the MLD-GA is $\mathcal{O}(|\mathcal{C}|^N)$ and increases exponentially with the number of antennas, the decision rule only requires the evaluation of simple weighted Euclidean distances. Also, the complexity of the MLD-GA depends on the order of the modulation scheme. Using an OOK modulation with $|\mathcal{C}| = 2$, the resulting complexity is $\mathcal{O}(2^N)$ which is reasonable for practical implementation. The implementation of the MLD-GA in practical systems would likely use a common digital signal processor. In contrast, the computational complexity of the NND depends mainly on the size of the used neural networks. Neural networks present high computational cost because they perform matrix multiplication. Hence, for a fully connected layer (dense), the order of the complexity is $\mathcal{O}(N_{in} \times N_n \times N_{out})$. In our case, for a 8×8 MIMO system, it leads to $\mathcal{O}(N_t^4)$, thus resulting in a computational complexity that may significantly exceed the one of MLD-GA. Regarding strict algorithm complexity, NND is more complex than the MLD-GA w.r.t. the demapping task. However, NND allows to perform "inner" channel estimation, which is complex to perform in our system model, and would be able to cope with additional nonlinear effects such as power amplifier non linearities. The proposed NND allows to show that with simple data, we can design a solution able to perform CSI estimation, detection and additional corrections. Besides, implementing neural network computations relies on very optimized algorithms [29] benefiting from cache usage, parallelism and shared memories [30]. For instance, fully connected layers may benefit from data and model parallelism, and pipelining; while in each layer, operations can be parallelized on either GPU or CPU. Besides, increasing the number of layers would drastically increase the complexity. Thereby, in our case, increasing the number of antennas will also increase the complexity of the NND. The complexity of both training and inference stages should be differentiated. Indeed, the training stage involves many data and consuming resources whereas the inference stage could be quite simple. Regarding the inference stage, it could be envisaged to quantize the NND weights to reduce resource usage and enhance energy efficiency. One may also consider pruning the neural networks to reduce the complexity, *i.e.* deactivate neurons with low valued weights and dead ones. Besides, the implementation of neural networks is currently a largely investigated research topic. Thus, implementing neural networks on dedicated hardware such as GPU, FPGA and ASIC can significantly decrease computation time regarding the chosen neural network architecture – readers may refer to [31] and [32]. It can be noted that in our system, GPU would be used for the calibration phase and a more energy efficient hardware for inference such as FPGA or ASIC. Moreover, an analog implementation of the decoder integrated to the analog front end, through spiking neural network [33] or the use of programmable discrete components [34] could help to reduce complexity and power consumption, especially to deal with very high data rate. However as we deal with digital transmission a one bit ADC is still necessary.

Last, it should be emphasized that in this work, for the contemplated applications such as device to device communication or indoor backhaul, it appears to be challenging to implement the proposed detectors in systems with $N \geq 16$ due to: i) the width of the antenna array, and ii) the complexity of the detector. However larger antenna system could be envisaged for other applications, e.g outdoor backhaul link.

3) Transceiver RF Nonlinearities: Eventually, it is interesting to mention that RF components of the transceiver might present additional nonlinearities, *e.g.* quantization, RF power amplifier. In particular, envelope detectors based on diodes may present non-ideal square law response such that $X_{\text{out}} \propto X_{\text{in}}^{\alpha}$ with $\alpha < 2$ [35]. It is expected that the NND might learn these channel nonlinearities and still demodulates symbol efficiently. The MLD-GA does not consider any other nonlinearities, such that it might be sensitive to these impairments and might require additional modeling. Nevertheless, it is of practical interest to characterize the detector robustness to imperfect RF components.

VI. Conclusion

We have investigated the design of MIMO systems with ED receivers for future applications in sub-THz bands. First, the system model has been described by characterizing the sub-THz channel and the RF architectures of the transmitter and receiver. Next, we have proposed two detection algorithms: i) the MLD-GA, derived from the ML decision rule for the studied nonlinear MIMO channel using a Gaussian approximation; ii) the NND, a detector based on the use of neural networks. Subsequently, a realistic scenario modeling an indoor wireless link has been considered to assess the communications performance. Simulation results have proved that low error rate communications can be achieved on strongly correlated LoS channels using the proposed detection schemes. The two proposed detectors present similar demodulation performance, yet their implementations in practical systems are very different. Moreover, we have shown that integrating a low-complexity channel coding scheme leads to valuable performance gains in terms of achievable data rate. In conclusion, our results demonstrate that spatial multiplexing with non-coherent sub-THz transceivers can be realized on strongly correlated LoS channels. Ultimately, the spectral efficiency of non-coherent communication systems using sub-THz bands can be efficiently increased using MIMO systems and ED receivers with low-complexity and low-power RF architectures.

Besides, it is worth mentioning that the presented techniques and results are relevant to applications beyond sub-THz communications such as visible light communications or optical systems. Visible light communication systems commonly implement intensity modulation and detection. The nonlinear interference between channels in these systems is also a major challenge to realize spatial multiplexing. The proposed detectors could be easily adapted to visible light communication systems in order to achieve spatial multiplexing.

Appendix

We derive here the probability distribution of received symbols expressed by Eq. (24). In detail, this paragraph intends to evaluate the distributions of the integrals in Eq. (24) expressed in the considered nonlinear MIMO channel of Eq. (7) by

$$\sqrt{2E_k[\tau]} \cdot w_k[\tau] = 2\int_{\tau T}^{\tau T+T} w_{k,c}(t)S_{k,c}(t) + w_{k,s}(t)S_{k,s}(t)dt \tag{24}$$

$$z_k[\tau] = \int_{\tau T}^{\tau T+T} w_{k,c}(t)^2 + w_{k,s}(t)^2 dt. \tag{25}$$

The following notations are used

$$S_{k,c}(t) = \sum_{n=1}^{N_t} h_{k,n}s_n(t)\cos\left(\varphi_{k,n} + \phi(t)\right),$$
$$S_{k,s}(t) = \sum_{n=1}^{N_t} h_{k,n}s_n(t)\sin\left(\varphi_{k,n} + \phi(t)\right). \tag{26}$$

It should be mentioned that in Eq. (8) the terms $w_k[\tau]$ and $z_k[\tau]$ respectively denote the mixed signal-noise contribution and the squared noise contribution in the channel. Under a strong oscillator phase noise assumption, we obtain

$$\int_{\tau T}^{\tau T+T} S_{k,c}(t)^2 dt = \int_{\tau T}^{\tau T+T} S_{k,s}(t)^2 dt = E_k[\tau]/2. \quad (27)$$

The strong oscillator phase noise assumption corresponds to $\int_T \cos(\phi(t))^2 \, dt = \frac{T}{2} + o(1)$. This assumption is verified for a fast varying phase noise (strong phase impairments). Nevertheless, if not the case, nothing but the variance of the mixed signal-noise term $w_k[\tau]$ is different, which has no further impact on the design of the detection algorithm. For this reason, this assumption results in no loss of generality. Signals $S_{k,c}(t)$, $S_{k,s}(t)$, $w_{k,c}(t)$ and $w_{k,s}(t)$ are band-limited and finite energy signals. With an observation of duration T and a band B, these signals lie in a signal space of dimension $2M = \lfloor 2BT \rfloor + 1$, see [22]. Hence these signals can be decomposed onto an orthonormal basis $\boldsymbol{\psi} = \{\psi_i\}_{1 \le i \le 2M}$ as follows

$$S_{k,c}(t) = \sum_{i=1}^{2M} S_{k,c}^i \cdot \psi_i(t), \quad S_{k,s}(t) = \sum_{i=1}^{2M} S_{k,s}^i \cdot \psi_i(t), \quad (28)$$

$$w_{k,c}(t) = \sum_{i=1}^{2M} w_{k,c}^i \cdot \psi_i(t), \quad w_{k,s}(t) = \sum_{i=1}^{2M} w_{k,s}^i \cdot \psi_i(t). \quad (29)$$

This decomposition enables us to derive the probability distribution of received symbols. It follows from Eq. (26) that the scalar coefficients of the decomposition verify

$$\sum_{i=1}^{2M} \left(S_{k,c}^i\right)^2 = \sum_{i=1}^{2M} \left(S_{k,s}^i\right)^2 = \frac{E_k[\tau]}{2}, \quad (30)$$

$$\mathrm{E}\left[\sum_{i=1}^{2M} |w_{k,c}^i|^2\right] = \mathrm{E}\left[\sum_{i=1}^{2M} |w_{k,s}^i|^2\right] = \frac{N_0 B}{2}, \quad (31)$$

where $\mathrm{E}[\cdot]$ is the expectation operator. Coefficients $w_{k,c}^i$ and $w_{k,s}^i$ are thus zero-mean Gaussian variables with variance $\sigma_w^2/2$. Let us recall that $\sigma_w^2 = N_0 B/2M$. By definition of basis $\boldsymbol{\psi}$, $\int_T \psi_i(t)\psi_j(t)dt = \delta_{ij}$. We are now in a position to express the distributions of the integrals in Eq. (24). First, for the mixed signal-noise contribution, the decomposition of the signals on basis $\boldsymbol{\psi}$ leads us to

$$\int_{\tau T}^{\tau T+T} w_{k,c}(t) S_{k,c}(t) dt = \sum_{i=1}^{2M}\sum_{j=1}^{2M} w_{k,c}^i S_{k,c}^j \int_{\tau T}^{\tau T+T} \psi_i(t)\psi_j(t) dt. \quad (32)$$

$$\int_{\tau T}^{\tau T+T} w_{k,c}(t) S_{k,c}(t) dt = \sum_{i=1}^{2M} w_{k,c}^i S_{k,c}^i \sim \mathcal{N}\left(0, \frac{E_k[\tau]}{4}\sigma_w^2\right). \quad (33)$$

Using similar derivations to evaluate $\int_T w_{k,s}(t) S_{k,s}(t) dt$, we obtain

$$\int_{\tau T}^{\tau T+T} w_{k,c}(t) S_{k,c}(t) + w_{k,s}(t) S_{k,s}(t) dt \sim \mathcal{N}\left(0, \frac{E_k[\tau]}{2}\sigma_w^2\right). \quad (34)$$

Second, for the squared noise contribution, we can express the integral as follows

$$\int_{\tau T}^{\tau T+T} w_{k,c}(t)^2 = \sum_{i=1}^{2M}\sum_{j=1}^{2M} w_{k,c}^i w_{k,c}^j \int_{\tau T}^{\tau T+T} \psi_i(t)\psi_j(t) dt,$$
$$\int_{\tau T}^{\tau T+T} w_{k,c}(t)^2 = \sum_{i=1}^{2M} (w_{k,c}^i)^2 \sim \sigma_w^2 \cdot \chi_{2M}^2. \quad (35)$$

With an identical reasoning on $\int_T w_{k,s}(t)^2 dt$, it finally appears that

$$z_k[\tau] = \int_{\tau T}^{\tau T+T} w_{k,c}(t)^2 + w_{k,s}(t)^2 dt \sim \frac{\sigma_w^2}{2} \cdot \chi_{4M}^2 \quad (36)$$

In summary, the received symbols are given by

$$r_k[\tau] = E_k[\tau] + \sqrt{2E_k[\tau]} \cdot w_k[\tau] + z_k[\tau], \quad (37)$$

where $w_k[\tau] \sim \mathcal{N}(0, \sigma_w^2)$ and $z_k[\tau] \sim \sigma_w^2/2 \cdot \chi_{4M}^2$.

REFERENCES

[1] S. Bicaïs, J.-B. Doré, and V. Savin, "Design of MIMO systems using energy detectors for sub-terahertz applications," in *Proc. IEEE Int. Symp. Pers., Indoor Mobile Radio Commun. (PIMRC)*, Sep. 2020, pp. 1–6.

[2] T. S. Rappaport *et al.*, "Wireless communications and applications above 100 GHz: Opportunities and challenges for 6G and beyond," *IEEE Access*, vol. 7, pp. 78729–78757, 2019.

[3] J.-B. Doré *et al.*, "Above-90 GHz spectrum and single-carrier waveform as enablers for efficient Tbit/s wireless communications," in *Proc. 25th Int. Conf. Telecommun.*, Saint-Malo, France, Jun. 2018, pp. 274–278.

[4] M. Voicu, D. Pepe, and D. Zito, "Performance and trends in millimetre-wave CMOS oscillators for emerging wireless applications," *Int. J. Microw. Sci. Technol.*, vol. 2013, pp. 1–6, Mar. 2013.

[5] J. L. Gonzalez-Jimenez *et al.*, "Channel-bonding CMOS transceiver for 100 Gbps wireless point-to-point links," *EURASIP J. Wireless Commun. Netw.*, pp. 1–21, 2020, Art. no. 117, doi: 10.1186/s13638-020-01741-1.

[6] S. Bicais and J.-B. Dore, "Design of digital communications for strong phase noise channels," *IEEE Open J. Veh. Technol.*, vol. 1, pp. 227–243, 2020.

[7] R. Combes and S. Yang, "An approximate ML detector for MIMO channels corrupted by phase noise," *IEEE Trans. Commun.*, vol. 66, no. 3, pp. 1176–1189, Mar. 2018.

[8] J. Park, S. Kang, S. V. Thyagarajan, E. Alon, and A. M. Niknejad, "A 260 GHz fully integrated CMOS transceiver for wireless chip-to-chip communication," in *Proc. Symp. VLSI Circuits (VLSIC)*, Jun. 2012, pp. 48–49.

[9] L. Jing, E. D. Carvalho, P. Popovski, and À. O. Martínez, "Design and performance analysis of noncoherent detection systems with massive receiver arrays," *IEEE Trans. Signal Process.*, vol. 64, no. 19, pp. 5000–5010, Oct. 2016.

[10] G. K. Psaltopoulos and A. Wittneben, "Diversity and spatial multiplexing of MIMO amplitude detection receivers," in *Proc. IEEE 20th Int. Symp. Pers., Indoor Mobile Radio Commun.*, Tokyo, Japan, Sep. 2009, pp. 202–206.

[11] T. O'Shea and J. Hoydis, "An introduction to deep learning for the physical layer," *IEEE Trans. Cogn. Commun. Netw.*, vol. 3, no. 4, pp. 563–575, Dec. 2017.

[12] H. Huang *et al.*, "Deep learning for physical-layer 5G wireless techniques: Opportunities, challenges and solutions," *IEEE Wireless Commun.*, vol. 27, no. 1, pp. 214–222, Feb. 2020.

[13] N. Farsad and A. Goldsmith, "Neural network detection of data sequences in communication systems," *IEEE Trans. Signal Process.*, vol. 66, no. 21, pp. 5663–5678, Nov. 2018.

[14] N. Samuel, T. Diskin, and A. Wiesel, "Deep MIMO detection," in *Proc. IEEE 18th Int. Workshop Signal Process. Adv. Wireless Commun. (SPAWC)*, Apr. 2017, pp. 1–5.

[15] N. Samuel, T. Diskin, and A. Wiesel, "Learning to detect," *IEEE Trans. Signal Process.*, vol. 67, no. 10, pp. 2554–2564, May 2019.

[16] M. Khani, M. Alizadeh, J. Hoydis, and P. Fleming, "Adaptive neural signal detection for massive MIMO," *IEEE Trans. Wireless Commun.*, vol. 19, no. 8, pp. 5635–5648, Aug. 2020.

[17] A. Elrharras, R. Saadane, M. Wahbi, and A. Hamdoun, "Hybrid architecture for spectrum sensing algorithm based on energy detection technique and artificial neural networks," in *Proc. 5th Workshop Codes, Cryptogr. Commun. Syst. (WCCCS)*, 2014, pp. 40–44.

[18] S. Verdú, "Spectral efficiency in the wideband regime," *IEEE Trans. Inf. Theory*, vol. 48, no. 6, pp. 1319–1343, Jun. 2002.

[19] L. Pometcu and R. D'Errico, "Characterization of sub-THz and mmWave propagation channel for indoor scenarios," in *Proc. 12th Eur. Assoc. Antennas Propag. (EurAAP)*, Apr. 2018, pp. 1–4.

[20] Y. Xing and T. S. Rappaport, "Propagation measurement system and approach at 140 GHz-moving to 6G and above 100 GHz," in *Proc. IEEE Global Commun. Conf. (GLOBECOM)*, Dec. 2018, pp. 1–6.

[21] G. Gougeon, Y. Corre, and M. Z. Aslam, "Ray-based deterministic channel modelling for sub-THz band," in *Proc. IEEE 30th Int. Symp. Pers., Indoor Mobile Radio Commun.*, Sep. 2019, pp. 1–6.

[22] P. Dollard, "On the time-bandwidth concentration of signal functions forming given geometric vector configurations," *IEEE Trans. Inf. Theory*, vol. IT-10, no. 4, pp. 328–338, Oct. 1964.

[23] J. Proakis, *Digital Communications* (Electrical and Computer Engineering: Communications and Signal Processing). New York, NY, USA: McGraw-Hill, 2007.

[24] S. Paquelet, L.-M. Aubert, and B. Uguen, "An impulse radio asynchronous transceiver for high data rates," in *Proc. Int. Workshop Ultra Wideband Syst. Joint with Conf. Ultra Wideband Syst. Technol.*, 2004, pp. 1–5.

[25] L. Barletta and G. Kramer, "On continuous-time white phase noise channels," in *Proc. IEEE Int. Symp. Inf. Theory*, Jun. 2014, pp. 2426–2429.

[26] D. P. Kingma and J. Ba, "Adam: A method for stochastic optimization," in *Proc. 3rd Int. Conf. Learn. Represent. (ICLR)*, Y. Bengio and Y. LeCun, Eds., San Diego, CA, USA, May 2015.

[27] F. F. Manzillo, A. Clemente, and J. L. Gonzalez-Jiménez, "High-gain *D*-band transmitarrays in standard PCB technology for beyond-5G communications," *IEEE Trans. Antennas Propag.*, vol. 68, no. 1, pp. 587–592, Jan. 2019.

[28] C. Fougstedt, K. Szczerba, and P. Larsson-Edefors, "Low-power low-latency BCH decoders for energy-efficient optical interconnects," *J. Lightw. Technol.*, vol. 35, no. 23, pp. 5201–5207, Dec. 1, 2017.

[29] S. Kestur, J. D. Davis, and O. Williams, "BLAS comparison on FPGA, CPU and GPU," in *Proc. IEEE Comput. Soc. Annu. Symp. VLSI*, May 2010, pp. 288–293.

[30] T. Ben-Nun and T. Hoefler, "Demystifying parallel and distributed deep learning: An in-depth concurrency analysis," *ACM Comput. Surv.*, vol. 52, no. 4, pp. 1–43, Sep. 2019.

[31] E. Nurvitadhi, J. Sim, D. Sheffield, A. Mishra, S. Krishnan, and D. Marr, "Accelerating recurrent neural networks in analytics servers: Comparison of FPGA, CPU, GPU, and ASIC," in *Proc. 26th Int. Conf. Field Program. Log. Appl. (FPL)*, Aug. 2016, pp. 1–4.

[32] E. Nurvitadhi, D. Sheffield, J. Sim, A. Mishra, G. Venkatesh, and D. Marr, "Accelerating binarized neural networks: Comparison of FPGA, CPU, GPU, and ASIC," in *Proc. Int. Conf. Field-Program. Technol. (FPT)*, Dec. 2016, pp. 77–84.

[33] A. Tavanaei, M. Ghodrati, S. R. Kheradpisheh, T. Masquelier, and A. Maida, "Deep learning in spiking neural networks," *Neural Netw.*, vol. 111, pp. 47–63, Mar. 2019.

[34] J. Kendall, R. Pantone, K. Manickavasagam, Y. Bengio, and B. Scellier, "Training end-to-end analog neural networks with equilibrium propagation," 2020, *arXiv:2006.01981*.

[35] *Square Law and Linear Detection*, Agilent Technologies, Santa Clara, CA, USA, 1999.

Simon Bicaïs received the M.Sc. degree in telecommunications from the National Institute of Applied Sciences of Lyon (INSA Lyon), France, in 2017, and the Ph.D. degree in signal processing and communication systems from the CEA-LETI, Grenoble, France, in 2020. He has been involved in the BRAVE national project about beyond 5G wireless communications in the Sub-TeraHertz bands. His current research interests include signal processing, wireless communications, and machine learning.

Alexis Falempin received the M.Eng. degree in telecommunications from the Institut Supèrieur d'Electronique de Paris, Paris, France, in 2019. He is currently pursuing the Ph.D. degree with the CEA-LETI, Grenoble, France. From September 2018 to December 2018, he was a Visiting Research Student at Cornell University, Ithaca, NY, USA. In November 2019, he joined the CEA-LETI. His current research interest includes the design of artificial intelligence solutions for wireless communications.

Jean-Baptiste Doré received the M.S. degree from the National Institute of Applied Sciences of Rennes (INSA), France, in 2004, and the Ph.D. degree in 2007. He joined NXP Semiconductors as a Signal Processing Architect. Since 2009, he has been with the CEA-LETI, Grenoble, France, as a Research Engineer and the Program Manager. He was involved in standardization group (IEEE1900.7). He has published more than 90 papers in international conference proceedings and book chapters and received three best papers awards. He is the main inventor of more than 30 patents. His main research topics are signal processing (waveform optimization and channel coding), hardware architecture optimizations (FPGA and ASIC), PHY, and MAC layers for wireless networks.

Valentin Savin received the dual M.S. degree in mathematics from the École Normale Supérieure, Lyon, and Joseph Fourier University, Grenoble, in 1997, and the Ph.D. degree in mathematics from Joseph Fourier University, in 2001. From 2002 to 2004, he was a Post-Doctoral Researcher with the Institute of Mathematics, Romanian Academy. Since 2005, he has been with the CEA-LETI, first as a two-year Post-Doctoral Researcher, and then as a Permanent Researcher. He has authored or coauthored about 100 scientific publications in peer-reviewed international journals, conference proceedings, and book chapters. His main research interests include various aspects of information and coding theory, including forward error correction for physical and upper layers applications, decoding algorithms and corresponding hardware architectures, decoding under faulty hardware, as well as the design of reliable systems built from unreliable components.